AIAA Infotech@Aerospace Conference
and
AIAA Unmanned...Unlimited Conference
6 - 9 April 2009, Seattle, Washington

AIAA 2009-1983

Wind Disturbance Estimation and Rejection for Quadrotor Position Control

Steven L. Waslander*, Carlos Wang†
University of Waterloo, Canada

The effect of wind on small quadrotor vehicle flight control can be quite significant, and can lead to dangerous situations when operating in close proximity to obstacles or other aerial vehicles. This work seeks to improve quadrotor positioning performance by formally modeling the wind effects on quadrotor dynamics in order to estimate wind velocities in flight and control the vehicle accordingly. Models for wind disturbances, quadrotor dynamics in wind and onboard measurements are presented and an estimation algorithm is developed for the current wind velocity experienced by the vehicle. This wind estimate is used to improve positioning accuracy by both eliminating the effect of wind on the feedback position control law and adding a wind compensator to mitigate the effect of the expected wind disturbance. Simulation results are presented for multiple scenarios, and work is ongoing for implementation on board a quadrotor testbed.

I. Introduction

Both fixed wing and rotary wing micro-aerial vehicles (MAVs) continue to increase in prevalence and are fast becoming more and more capable. Specific advantages drive this trend, including the low relative cost of construction and the ability to operate in dense environments with limited space for maneuvering. Often, MAVs use electric propulsion systems, resulting in low maintenance requirements and significantly reduced potential for damage in the event of failure. If a task can be completed by a MAV, there is no point sending a more expensive, dangerous and cumbersome vehicle.

The applications that arise for MAVs, therefore, often involve operations in environments that include a large percentage and varied type of obstacles. To operate in such environments in a safe and controlled manner, it is essential to better understand the varied wind conditions affecting position and trajectory tracking. Direct modeling of 3D wind environments is a time consuming and laborious task in computational fluid dynamics, for which online solvers that could be incorporated onto MAVs do not exist. This work seeks to find appropriate methods for MAVs to gain enough insight from simple estimation algorithms to enable safe operation in varying and various wind conditions.

Specifically, the case of quadrotor helicopter operation in urban environments is taken as a test case with sufficient challenges to validate the proposed techniques. Applications for which quadrotors are envisaged include bridge and building inspection, fire safety and coordinated compound surveillance as an augmentation system for a base set of fixed cameras. More complex environments arise in applications such as search and rescue operations in forested areas, indoor operation for reconnaissance in unsafe buildings and advanced fire detection in warehouses. Although the indoor environments are unlikely to contain strong winds, the vehicle downwash when operating so close to walls and floors can have a similar impact on vehicle performance.

The notion of understanding wind characteristics for the benefit of unmanned aerial vehicle (UAV) guidance and navigation is not new. Much work has been done on large scale phenomena such as thermal soaring,[1] ridge soaring,[2] and exploitation of wind gusts.[3–5] In each case, the environments in which these

*Steven Waslander is an Assistant Professor in the Department of Mechanical and Mechatronics Engineering at the University of Waterloo, Waterloo, ON, Canada. email: stevenw@uwaterloo.ca.

†Carlos Wang is a Masters student at the University of Waterloo, Waterloo, ON, Canada. email: c25wang@engmail.uwaterloo.ca.

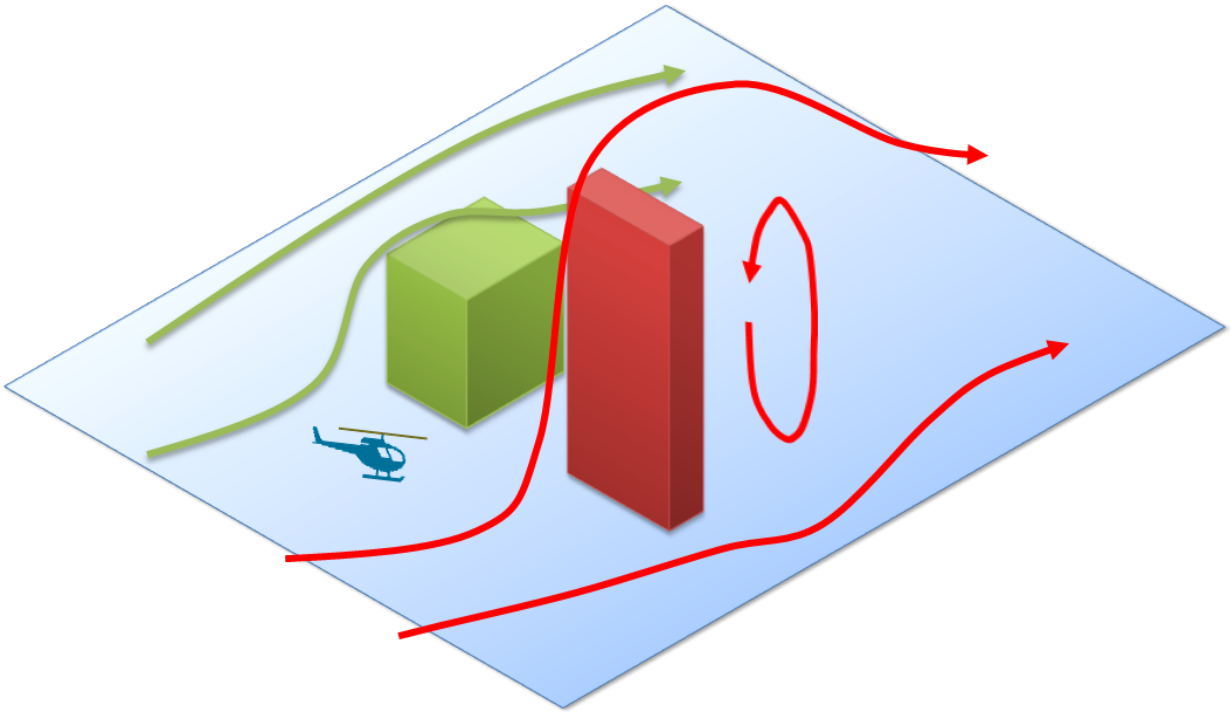

Figure 1. Micro-aerial vehicle missions include operation in urban environments in close proximity to large obstructions to the dominant wind direction, which result in large turbulent airflow patterns for which accurate prediction is not possible with limited resources.

conditions are studied are relatively benign and devoid of obstacles. As a result, assumptions such as constant wind fields are often used[5] and long time scale phenomena have been more closely considered. The reason for these assumptions is primarily that short term, turbulent wind effects are difficult to model even with detailed CFD analysis, and this approach is impractical from a control standpoint.

The difficulty of predicting wind patterns for MAV flight in urban environments is well documented,[6] and remains a vibrant area of ongoing research. This work seeks to design controllers which make use of simple estimates of current wind velocity to provide a controller that reduces the impact of wind disturbances on vehicle positioning accuracy. The wind estimates are derived from vehicle accelerometer measurements which are affected by all forces acting on the vehicle, excluding gravity. Relying on previous work which successfully identified aerodynamic effects of altitude control for the Stanford Testbed of Autonomous Rotorcraft for Multi Agent Control (STARMAC),[7] it is possible to isolate the effects of wind disturbances from the other forces acting on the vehicle for control. Instead of then considering a dynamic model for wind velocity propagation, the approach relies on the assumption that the time scale of wind variations is slow compared to the sampling frequency of accelerometer measurements.

The main contributions of this work include a derivation of the effect of wind on the quadrotor dynamics models previously developed in earlier work, the presentation of a straight-forward wind velocity estimation algorithm which relies exclusively on onboard data and a controller design that improves overall system performance with the use of short time frame wind estimation. The results are presented in simulation only, although work is ongoing to implement the controller onboard the Aeryon Scout quadrotor helicopter, a new design from Aeryon Labs Inc. located in Waterloo, Canada.[8]

This paper proceeds as follows. Section II presents the main elements of the problem formulation. The vehicle dynamics are described in detail, as are the sensors and sensor models assumed to be available. Wind modeling is then presented, and relies on both temporal models such as the Dryden wind gust model[9] and spatial variation due to boundary layer effects to generate a realistic wind field. In Section III, the simplifications used to enable onboard wind velocity estimation from accelerometer data are presented, and Section IV continues with the feedback control approach applied. Simulation results for three separate control options are presented in the penultimate section, and concluding remarks along with some desirable

Figure 2. Two quadrotor vehicles from The Stanford Testbed of Autonomous Rotorcraft for Multi-agent Control (STARMAC) in autonomous hover operation.

avenues for future work are discussed in Section VI.

II. Problem Formulation

The problem under consideration can be described as follows: Given the availability of acceleration data onboard a quadrotor vehicle, is it possible to estimate current wind disturbance conditions, reliably predict subsequent wind disturbances and determine control actions that correct for these expected disturbances? The problem requires a detailed dynamic model of the vehicle which includes the effect of freestream velocity on forces and moments experienced by the vehicle. It also requires a compact model of expected wind disturbances, and an understanding of the effect of wind conditions on the vehicle. Instead of simply reacting to disturbances once they produce a measurable result in terms of position, velocity and acceleration error, the goal is to eliminate the effect of wind disturbances by predicting them as they occur.

A. Vehicle Dynamics Modeling

Coordinate systems and reference vectors for the problem of interest are defined in Figure 3-a), including the inertial frame (I) in North, East, Down $(\hat{\mathbf{n}}, \hat{\mathbf{e}}, \hat{\mathbf{d}})$ and the body fixed frame (B) with origin at the vehicle center of gravity $(\hat{\mathbf{x}}, \hat{\mathbf{y}}, \hat{\mathbf{z}})$. Euler angles of roll, pitch and yaw (ϕ, θ, ψ) define a rotation matrix R_I^B for rotation from inertial to body coordinates through three successive rotations in standard (3,2,1) form.[10] The freestream velocity v_∞ and direction $\hat{\mathbf{e}}_\infty$ are also depicted, which are the magnitude and direction of the combination of the wind velocity $\mathbf{v_w}$, and the vehicle velocity, $\mathbf{v_I}$, both in the inertial frame. The direction of the freestream velocity is broken into components $\hat{\mathbf{e}}_\mathbf{h}$, parallel to the rotor plane and $\hat{\mathbf{e}}_\mathbf{v}$ perpendicular to it. Lastly, Figure 3-a) presents a clockwise rotor numbering scheme for the quadrotor vehicle, with rotor 1 along the positive $\hat{\mathbf{x}}$ axis, and rotor 2 along the positive $\hat{\mathbf{y}}$ axis, etc.

A free body diagram of the quadrotor vehicle is depicted in Figure 3-b). The forces and moments considered for each rotor are visible for each rotor (vertical (T_i, Q_i) and longitudinal (D_i, P_i) relative to the direction of the freestream), and are labeled for rotor 1 only to avoid unnecessary clutter. In fact, both lateral forces and moments are also produced by each of the rotors during most flight regimes, but since quadrotors consist of two sets of counter-rotating pairs of rotors, these lateral effects tend to cancel and can be safely omitted from the analysis. Also visible in Figure 3-b) are the body drag force, D_B and the

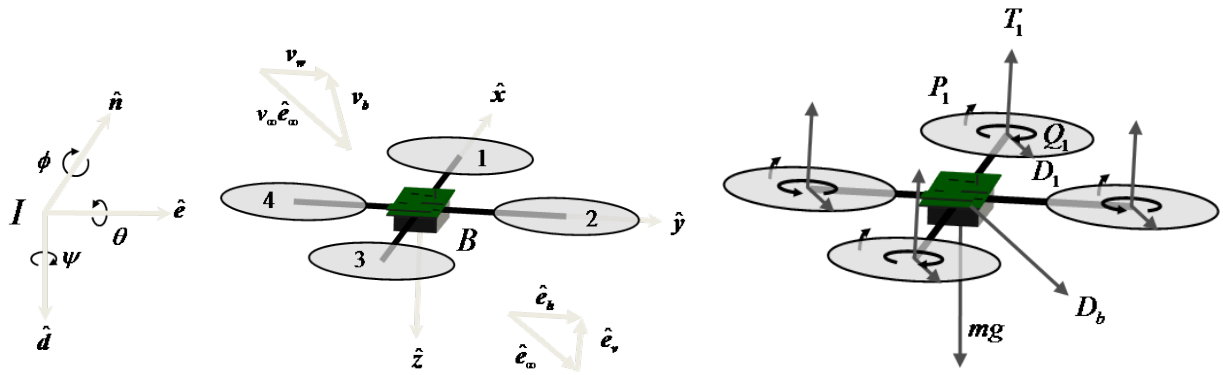

a) b)

Figure 3. a) Coordinate system for vehicle dynamics definitions and b) free body diagram of quadrotor in the freestream.

gravitational force (mg) acting on the vehicle.

The complete set of forces and moments acting on the vehicle can be summarized as follows, expressed in body coordinates:

$$\mathbf{F}_B = \sum_{i=1}^{4}(-T_i\hat{\mathbf{z}} + D_i\hat{\mathbf{e}}_\infty) + D_B\hat{\mathbf{e}}_\infty + R_I^B mg\hat{\mathbf{d}}, \tag{1}$$

$$\mathbf{M}_B = (Q_1 + Q_3 - Q_2 - Q_4)\hat{\mathbf{z}} - \sum_{i=1}^{4}(P_i\mathbf{e_t} + D_i(\mathbf{r_i} \times \hat{\mathbf{e}}_\infty) + T_i(\mathbf{r_i} \times -\hat{\mathbf{z}})). \tag{2}$$

where $\mathbf{r_i}$ defines the vector from the center of gravity to the center of rotation of each rotor i, and $\mathbf{e_t}$ defines the direction perpendicular to the freestream direction in the rotor plane. The combination of forces and moments acting on the vehicle result in the following dynamic equations of motion, where subscripts I and B denote the coordinate frame, p_I is inertial position, v_I is inertial velocity, the Euler angles are denoted Θ with body angular rates ω_B and J is the moment of inertia matrix for the vehicle.

$$\dot{p}_I = v_I \tag{3}$$
$$v_I = R_B^I v_b \tag{4}$$
$$\dot{v}_B = \frac{1}{m}F_B - \omega_B \times v_B \tag{5}$$
$$\dot{\Theta} = R_E\omega_B \tag{6}$$
$$\dot{\omega}_B = J^{-1}M_B - \omega_B \times J\omega_B \tag{7}$$

The Euler rotation matrix, R_E, follows conventional definition[10] and converts body angular rate measurements to Euler angle rates of change.

The key difficulty in the modeling of quadrotor vehicle dynamics lies in expressing the forces and moments acting on the vehicle in terms of the vehicle velocity relative to the free stream. Relying on existing work on quadrotor aerodynamics,[7] which develops thrust and moment relations from blade flapping and momentum theory using helicopter research,[11] the thrust for each rotor can be concisely expressed as

$$T_i = C_\infty(\alpha, v_\infty, v_i)C_h V_i^2, \tag{8}$$

where V_i is the voltage applied to the motor, C_h is the coefficient of thrust at hover conditions, and $\frac{T_i}{T_h} = C_\infty$ is the ratio of thrust, T_i produced with angle of attack α, freestream velocity v_∞ and induced velocity v_i to the thrust produced at hover, T_h for the same applied voltage to the motor. Note that this model of rotor thrust is a steady state model, and does not include dynamic effects for rotor response. The angle of attack $\alpha = f_\alpha(v_\infty, \Theta)$ defines the angle between the vehicle body $x-y$ plane and the freestream velocity. The induced velocity defines the change in airspeed across the rotor plane, and is modeled differently depending

on flight conditions, but is a function of the freestream velocity, angle of attack and voltage applied to the motor (which determines the induced velocity in hover conditions). Therefore, the thrust ratio relation can be rewritten as,

$$\frac{T_i}{T_h} = C_\infty(v_\infty, \Theta, V_i) \tag{9}$$

In addition to the change in magnitude of the thrust produced, there is also an effect that results in a change in the direction of the thrust vector, away from the $\hat{\mathbf{z}}$ axis. This is the result of blade flapping, which is caused by an imbalance in thrust produced on the advancing and retreating blades. Only very small deflections occur as a result of this phenomenon, and so small angle approximations can be used. Due to the counter-rotating pairs of blades, lateral forces that are produced by this effect cancel, and only the longitudinal effects need be considered. The result is a longitudinal thrust component which can be summed for all four rotors, T_l, and is linearly dependent on the freestream velocity as follows,

$$T_l = K_{bf} v_\infty \cos\alpha \tag{10}$$

where K_{bf} is the coefficient of blade flapping. This longitudinal force acts in the $\hat{\mathbf{e}}_\mathbf{h}$ direction, and can also result in a moment if the rotor plane is not vertically aligned with the vehicle cg. For more details on the derivation of Equation 8, Equation 10 and on the relation C_∞, please refer to previous work by Hoffmann et al.[7]

Drag on the body and the rotor drag forces can be modeled simply as a single force in the inertial frame, D, resistive to forward motion and related linearly to the magnitude of the freestream velocity,

$$D = C_D v_\infty, \tag{11}$$

where C_D is an aggregated coefficient of drag which can be experimentally determined. Although drag can be modeled more accurately as quadratically dependent on velocity and rotor drag can be more precisely modeled when the applied voltage is also considered, in practice, this added complexity adds little in terms of accuracy of the model. Linearization about a nominal speed is included in the definition of C_D.

The moments generated by the voltage inputs V_i are similarly summarized from previous work, and result in the following relationships. The aerodynamic torque required to generate the thrust for each motor

$$Q_i = C_\tau V_i^2, \tag{12}$$

where C_τ is an aggregated coefficient of torque. The torque at each rotor is not affected by freestream velocity in the same manner as rotor thrust. The longitudinal moments are a result of blade flapping, and are modeled as

$$M_l = \sum_{i=1}^{4} P_i = \tilde{K}_{bfm} v_\infty \cos\alpha + T_l(r_i \times \hat{\mathbf{e}}_\mathbf{h}) = \kappa_{bfm} v_\infty \cos\alpha \tag{13}$$

where κ_{bfm} is an aggregate coefficient of blade flapping moments, combining the moment resulting from the deflection of fixed blades with the moment produced by the deflection of the thrust vector. Here, $\tilde{K}_{bfm}$ is the constant coefficient relating the blade flap angle to the resulting moment produced. The total longitudinal moment, M_l, results in a pitch up effect in nonzero freestream conditions.

B. Vehicle Measurement Modeling

The quadrotor is assumed to have the following measurements of its state: GPS for position, p_I, and velocity, v_I, at 10 Hz with $\pm 2-5$ cm accuracy in x-y position and $\pm 4-10$ cm accuracy in height (carrier phase differential GPS), 3-axis accelerometer, magnetometer and gyro measurement at 50 Hz for body acceleration, a_B, magnetic field direction, μ_B and angular velocity, ω_B, with ± 0.3 g, ± 2 ° and ± 0.1 °/s accuracy, respectively. A barometric pressure sensor is used for height measurements, d_b with ± 30 cm accuracy, as well as sonic ranging for height above the ground, z_g with $\pm 2-5$ cm accuracy and a range of 1.5 meters. Although these assumptions are rather specific and reflect the capabilities of a specific quadrotor design, the results from this work can be readily adapted to other measurement scenarios.

The magnetometers provide a magnetic field direction in inertial coordinates, μ_I, to be detected on the vehicle which can be assumed constant for the application of interest,

$$\mu_B = R_I^B \mu_I. \tag{14}$$

Accelerometers measure the total forces acting on the vehicle, with the exception of the gravitational field. In free fall, all three axes of the accelerometers would measure zero, and so the actual in-flight measurements include all forces other than gravity as follows. Let A_B be the accelerometer measurements in the body frame, then

$$a_B = \frac{1}{m}\left(\sum_{i=1}^{4}(T_i\hat{\mathbf{z}}) + T_l\hat{\mathbf{e}}_{\mathbf{h}} + D\hat{\mathbf{e}}_\infty - \omega_B \times (\omega_B \times r_A) - \dot{\omega}_B \times r_A\right), \tag{15}$$

where r_A is the vector from the CG to the location of the accelerometers in body coordinates. The above equation allows for the fact that the accelerometers are not located at the CG and therefore experience centripetal accelerations due to angular velocities of the vehicle. In practice this is a negligible effect (for the vehicle of interest, accelerometers were under 2cm from the CG). A simplified model for the accelerometer measurements is

$$a_B = \frac{1}{m}\left(\sum_{i=1}^{4} C_\infty(v_\infty, \Theta, V_i)C_h V_i^2\hat{\mathbf{z}} + R_I^B\left(K_{bf}v_\infty \cos\alpha\hat{\mathbf{e}}_{\mathbf{h}} + C_D v_\infty \hat{\mathbf{e}}_\infty\right)\right), \tag{16}$$

Note that a typical fixed wing simplifying assumptions for the accelerometers, whereby the accelerometer measurements are assumed to indicate the direction of gravity, lead to inaccurate models for inertial measurement unit (IMU) based Euler angle estimation in rotorcraft, and are not used here.

It is now possible to define the base vehicle measurement model. A state vector can be defined as

$$x^T = [p_I \quad v_B \quad \Theta \quad \omega_B], \tag{17}$$

where each element is in fact a vector with three components, resulting in 12 states. The control inputs are

$$u^T = [V_1 \quad V_2 \quad V_3 \quad V_4]. \tag{18}$$

A standard extended Kalman filter (EKF)[12] is used to combine the above measurements into state estimates, based on the dynamics defined in Equation (7), denoted $\dot{x} = f(x, u)$, and the following measurement model:

$$y = h(x, u, v_w) = \begin{bmatrix} p_I \\ R_B^I v_B \\ \text{Eqn (16)} \\ \text{Eqn (14)} \\ \omega_B \\ -d \\ d_{ref} - d \end{bmatrix}. \tag{19}$$

where d is the altitude in inertial coordinates d_{ref} is the ground level altitude. A key difficulty remains with the measurement model as defined here, and is related to the complex nonlinear relationship that defines the accelerometer thrust model. In practice, it is difficult to linearize the equations for thrust and so a simplification is often employed which neglects the dependence of thrust produced on the freestream velocity. This assumption results in reasonable estimates for low speed operations, but may result in divergence when the accelerometer measurements vary significantly from what might be expected from the model. This issue remains an area of ongoing investigation.

C. Wind Modeling

The wind modeling used in this work consists of two main components, a static dominant wind direction and strength model and a wind gust model dependent on a standard power spectral density (PSD). The static component which characterizes the underlying dominant wind characteristics can be initialized with meteorological observations from a base station and is presumed to vary on a time scale somewhat larger than the scale of vehicle flight time. The wind gust model with accompanying PSD is derived from the Dryden model,[13] relying on the static wind model to generate necessary parameters for the PSD.

For the static model, wind velocity $\mathbf{v_w}$ is assumed to be constant throughout the flight. An altitude dependence for magnitude of mean wind velocity is included to account for boundary layer effects in open terrain,

$$v_w(z) = \frac{1}{k}v_w^* \ln\left(\frac{z}{z_0}\right), \tag{20}$$

where z is the height of the quadrotor from the earth's surface, z_0 is the roughness length, k is the von Kármán constant, v_w^* is the friction velocity from the earth's surface, and $v_w(z)$ is taken to be the wind velocity at height z. Values of $k = 0.4$ and $z_0 = 0.05$ were used, representing typical values for open terrain.[14] Given values of $v_w(z)$ and z from flight data, v_w^* can be determined by solving Equation 20.

The upper limit $\bar{z}$ for which Equation (20) is valid is

$$\bar{z} = b\frac{v_w^*}{2\omega_e \sin\phi_l}, \tag{21}$$

where b is a scaling constant (between 0.015 and 0.030, 0.02 in this work),[14] ϕ_l is the earth's latitude for the given location, and ω_e is the angular speed of the earth on the north-south axis. The previous two equations are used to determine the magnitude of the mean wind velocity at a given height within the boundary layer on the earth's surface.

The Dryden wind gust model is defined as a summation of sinusoidal excitations,

$$v_w(t) = v_w^0 + \sum_{i=1}^{n} a_i \sin(\Omega_i t + \varphi_i), \tag{22}$$

where $v_w(t)$ is a time-dependent estimate of the wind vector given time t, Ω_i and φ_i are randomly selected frequencies and phase shifts, n is the number of sinusoids, a_i is the amplitude of the sinusoid, and v_w^0 is the ambient wind vector (or static wind vector). The values of Ω_i are taken between 0.1 to 1.5 rad/s.

The magnitudes a_i are given by

$$a_i = \sqrt{\Delta\Omega_i \Phi(\Omega_i)}, \tag{23}$$

where $\Delta\Omega_i$ are the intervals between the frequencies and $\Phi(\Omega_i)$ is the power spectral density (PSD). The PSD for vertical wind and horizontal winds are different and are found from the following equations.

$$\Phi_h(\Omega) = \sigma_h^2 \frac{2L_h}{\pi} \frac{1}{1 + (L_h\Omega)^2} \tag{24}$$

$$\Phi_v(\Omega) = \sigma_v^2 \frac{L_v}{\pi} \frac{1 + 3(L_v\Omega)^2}{(1 + (L_v\Omega)^2)^2} \tag{25}$$

Here, σ_h and σ_v are the horizontal and vertical turbulence intensities, L_h and L_v are the horizontal and vertical gust length scales. The vertical length scale and turbulence intensity can be assumed to be $L_v = |z|$, $\sigma_v = 0.1\omega_{20}$ (ω_{20} is the given wind speed in knots at 20 ft altitude). These relations are valid for altitudes below 1000 ft.[13] Finally, L_h and σ_h can be found with the following equations:

$$\frac{L_h}{L_v} = \frac{1}{(0.177 + 0.000823z)^{1.2}}, \tag{26}$$

$$\frac{\sigma_h}{\sigma_v} = \frac{1}{(0.177 + 0.000823z)^{0.4}}. \tag{27}$$

The wind field model therefore defines the wind speed at a given altitude, and varies both temporally and spatially (in altitude).

III. Wind Estimation

The only manner available for determining the wind velocity relies on the use of the accelerometer data. The total forces acting on the vehicle in zero freestream conditions are understood, and any deviations from the accelerations that should result given the current state and inputs can be primarily attributed to wind disturbances. Two simplifications are needed to form a tractable wind velocity estimate. First, it is impractical to attempt to utilize the full Dryden wind gust model to estimate gust dynamics. Instead, wind estimation is done in a memoryless manner, ignoring the previous wind state estimate although in future it would be trivial to add low pass filtering to capture the low bandwidth of wind gust variations. Second, the dependence of the $\hat{\mathbf{z}}$ axis thrust equation on wind velocity does not afford the possibility of direct inversion. Therefore, for this specific component of thrust, it is assumed that the wind velocity does not change significantly over one time step, and the previous value, $\tilde{v}_w$ is used. The estimation of wind

velocity is memoryless, but the previous wind velocity estimate is used to predict the thrust currently being generated. In both cases, a reliance on low bandwidth variation in wind is used to justify the assumptions.

The approach relies on inversion of the equations that define the components of the accelerometer measurements. The state vector is augmented to include wind velocity, v_w, and the accelerometer measurement model is modified to distinguish the contributions to drag from both vehicle and wind velocity.

$$a_B = \frac{1}{m}\left(\sum_{i=1}^{4} C_\infty(v_I - v_w, \Theta, V_i) C_h V_i^2 \hat{\mathbf{z}} + R_I^B \left(K_{bf}(v_I - v_w)\cos\alpha \hat{\mathbf{e}}_\mathbf{h} + C_D(v_I - v_w)\hat{\mathbf{e}}_\infty\right)\right) \tag{28}$$

Ideally, the wind velocity would be isolated from this equation allowed for estimation through inversion of the measurement equation. However, the function C_∞ is implicitly a fourth order function of v_w, making such an inversion difficult. Instead, the thrust dependence on wind velocity is decoupled and it is possible to rewrite Equation 28 as,

$$a_B = \frac{1}{m}\left(\sum_{i=1}^{4} C_\infty(v_I - \tilde{v}_w, \Theta, V_i) C_h V_i^2 \hat{\mathbf{z}} + R_I^B \left(K_{bf}(v_I - v_w)\cos\alpha \hat{\mathbf{e}}_\mathbf{h} + C_D(v_I - v_w)\hat{\mathbf{e}}_\infty\right)\right) \tag{29}$$

essentially taking drag and blade flapping effects as the only effects to be considered for wind estimation. Although this may seem to be a significant assumption, in practice the sole effect is to cause erroneous vertical wind estimation components, which have very little impact on the horizontal control proposed in Section IV. Solving this equation for the wind velocity v_w yields,

$$v_w = \frac{1}{K_{bf}\cos\alpha\hat{\mathbf{e}}_\mathbf{h} + C_D\hat{\mathbf{e}}_\infty} R_B^I \left(\sum_{i=1}^{4} C_\infty(v_I - \tilde{v}_w, \Theta, V_i) C_h V_i^2 \hat{\mathbf{z}} - m a_B\right) + v_I. \tag{30}$$

which can be computed based on measured body accelerations and inertial velocities, angles determined from the EKF, the previous wind velocity estimate and the thrust model derived in Section II. Unlike the EKF formulation in Section II, it is possible to include the aerodynamic effects of non-zero freestream velocity in the thrust calculations because the dependence on v_w has been removed through a zero-order hold and modeled effects are simply subtracted from the accelerometer measurements.

IV. Controller Approach

Previous work in quadrotor horizontal position control has demonstrated the merits of PID control with an added term for acceleration rejection (referred to as double derivative (DD) control).[7] This work focused primarily on zero wind conditions, and so the DD term was used to add damping to the system in benign conditions and improve tracking performance. Since the actuation of position in the North and East directions is through the components of thrust in those directions caused by roll and pitch angles, the DD term acts to restore the vehicle to zero tilt. In windy conditions, however, the ideal tilt may not be zero, and so a wind compensator is added to the outer position control loop to correct for the wind effects.

The compensation term to account for wind disturbances, u_F, is computed by assuming the current measured wind will persist in the short term (until the next measurement). This assumption is used to relax the need for accurate determination of the complex wind dynamics in real time. In effect, zero dynamics are used for the wind. For small disturbances, it is possible to assume small angle commands will be required. The drag forces caused by the wind can be canceled by adding a sufficient angle, $\delta\phi, \delta\theta$, to the pitch and roll commands. For a given total thrust, $T_t = \sum_{i=1}^{4} T_i$, these forces are balanced if,

$$R_B^I T_t \hat{\mathbf{z}} \sin\phi = \left(K_{bf}\cos\alpha + C_D(v_w)\right) v_w \tag{31}$$

Since the wind velocity is a vector in the inertial frame, the wind compensator command is also a vector with NED components. The third element is then set to zero, and the first two are rotated about the yaw axis to provide pitch and roll offsets that will counteract the accelerations caused by the wind which is added to the roll and pitch commands that result from the feedback controller. Incorporating small angle assumptions, the angle requests are,

$$\begin{bmatrix} \delta\phi \\ \delta\theta \\ 0 \end{bmatrix} = R_\psi \frac{\left(K_{bf}\cos\alpha + C_D\right) v_w}{T_t} \tag{32}$$

The angles $\delta\phi, \delta\theta$ are then added to the roll and pitch requests from the PID,DD controller that governs the outer loop. Note that the estimate of thrust in the controller relies on the updated wind velocity estimate.

V. Simulation Results

The results are demonstrated on a full nonlinear simulation of the quadrotor vehicle, which includes inner loop attitude and altitude control, outer loop position control, and dynamics which incorporate aerodynamic effects based on freestream velocity. A simple hover scenario is depicted in the figures in this section to get a sense for the relative performance of the various controllers proposed. In each case, the simulation represents 30 seconds of flight time with a goal location of (0,0,2) in ENU coordinates for easier visualization. All variations in position are simply the result of sensor noise, wind disturbances, discretization, time delay and vehicle dynamics.

In Figure 4, the wind disturbances and resulting estimates of wind velocity from accelerometer data are compared, demonstrating the possibility of extracting wind velocity estimates from accelerometer data.

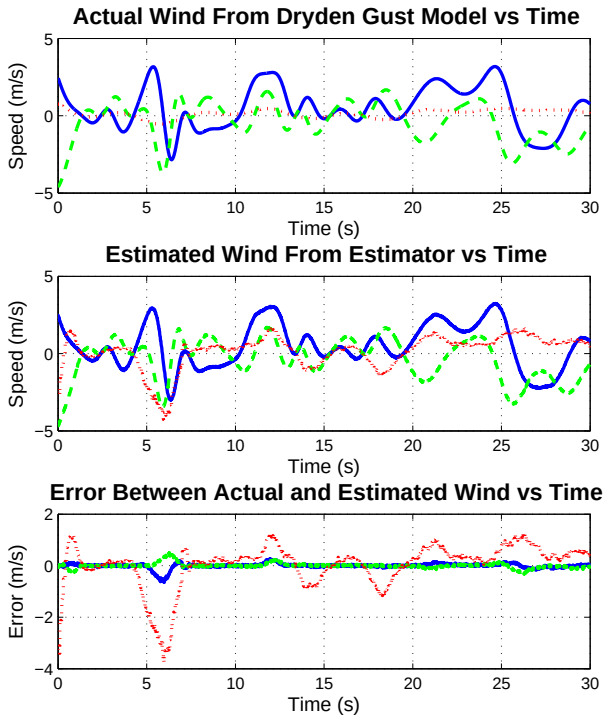

Figure 4. Wind velocity in inertial coordinates that results from the Dryden wind gust model, the estimates of wind velocity that result from the estimation algorithm and the errors between actual and observed wind velocity. The three wind components are presented: North (blue solid), East (green dashed) and Down (red dotted).

As a baseline for comparison, a tuned PID controller was implemented and a hover simulation was performed in the above wind field. Errors range in the ± 0.4 m region, which is reasonably consistent with outdoor flight test results.

Applying the same wind disturbances, the advantage of the added DD term in the position control accuracy can be observed in Figure 6 over standard PID control. The range of errors reduces to ± 0.15 m, showing a significant improvement over the PID control in Figure 5.

Finally, the additional improvement of adding the wind compensation term to the control law is presented in Figure 7. Errors are further reduced to a ± 0.1 m range, which is comparable to indoor flight test in the

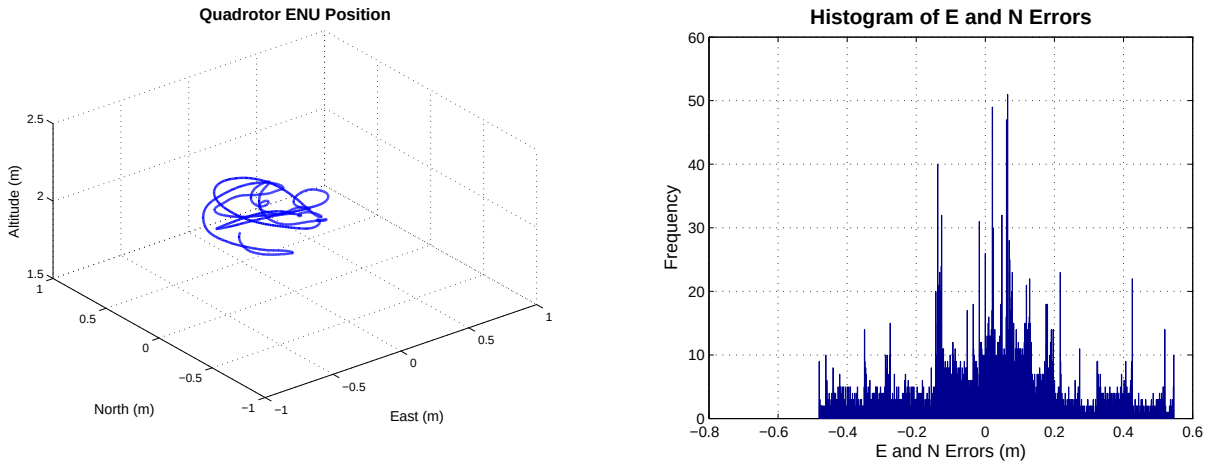

a) b)

Figure 5. Hover performance with PID control, a) vehicle motion in three dimensions, b) histogram of errors in the horizontal plane (north,east).

absence of wind disturbances for this type of vehicle, although it is premature to suggest such results would be achievable on real vehicles.

These results clearly indicate the potential of the method proposed, although more detailed analysis and implementation on testbed vehicles will significantly improve the validity of conclusions drawn from these results. Similar results are possible when the vehicle velocity is non-zero. In the following two scenarios, linear (Figure 8) and circular (Figure 9) trajectories are flown through a varying wind field, and tracking performance is not significantly reduced over the hover flight conditions. In both cases, a significant initial deviation occurs, which results in the long tail and skewed error histogram in both cases. This initial deviation is caused by aggressive inputs to adjust to desired initial conditions requiring vehicle motion.

VI. Conclusions and Future Work

This work seeks to develop a methodology for mitigating the effects of winds on small aerial vehicle platforms, and in particular for the unique dynamics of quadrotor vehicles. Despite the complexity of the nonlinearities involved in this process, the approach of measurement equation inversion for onboard estimation of wind velocity to then be applied to position control appears to hold promise when considering the simulation results presented in Section V. This approach hinges on numerous simplifications on order to become tractable, which bodes well for the feasibility of implementation, but poorly for the accuracy of the simulation results with respect to real world behavior of quadrotors.

Much remains to be explored, and in particular, this work will benefit from field tests in measured wind conditions. The simulation environment allows for too much clarity on parameters that significantly affect the dynamics of the vehicle, such as the coefficient of drag, and zeroed accelerometer biases. In experimentation on board the vehicle, in fact, it was not possible to get sufficient clarity on the correspondence between observed wind data and the accelerometer measurements, an area of concerted future efforts.

Improved estimation techniques must also be considered, the most obvious of which would be to include additional states and the measurement model for wind velocity in the onboard EKF. As a proof of concept however, the method presented here provides an interesting first step toward wind disturbance rejection for quadrotor vehicles.

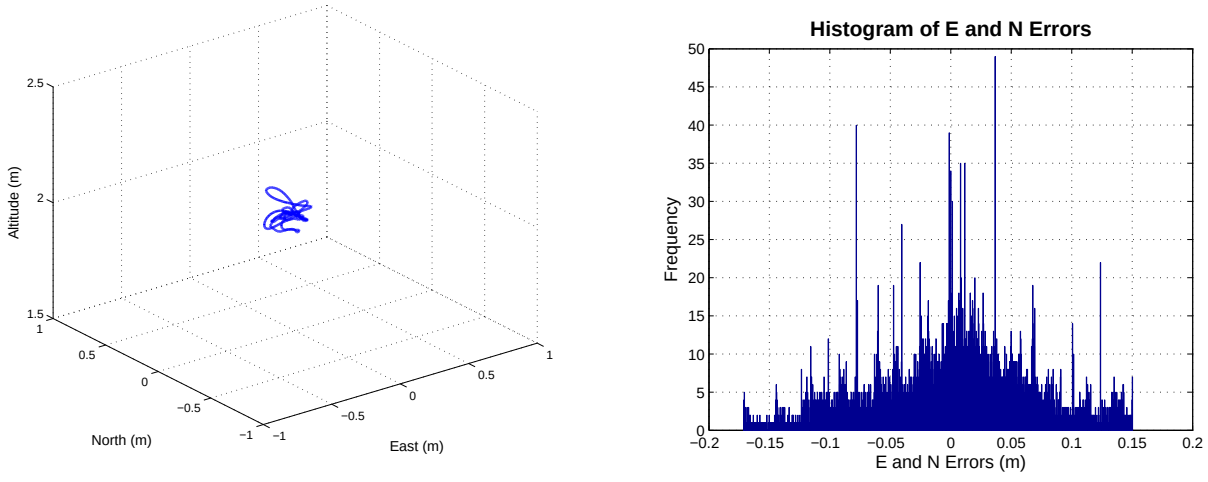

a) b)

Figure 6. Hover performance with PID,DD control, a) vehicle motion in three dimensions, b) histogram of errors in the horizontal plane (north,east).

Acknowledgements

The authors would like to thank Mike Peasgood and April Deirdre Blaylock of Aeryon Labs Inc. for their helpful contributions to this work, and for the many stimulating conversations concerning estimation and control of quadrotor helicopters.

References

[1]Allen, M., "Autonomous Soaring for Improved Endurance of a Small Uninhabitated Air Vehicle," *43rd AIAA Aerospace Sciences Meeting and Exhibit*, Reno, Nevada, January 2005.

[2]Langelaan, J. W., "Long Distance/Duration Trajectory Optimization for Small UAVs," *AIAA Guidance, Navigation and Control Conference and Exhibit*, Hilton Head, South Carolina, August 2007.

[3]Boslough, M. B. E., "Autonomous Dynamic Soaring Platform for Distributed Mobile Sensor Arrays," Tech. rep., 2002.

[4]Patel, C. K. and Kroo, I., "Control Law Design for Improving UAV Performance Using Wind Turbulence," *44th AIAA Aerospace Sciences Meeting and Exhibit*, No. AIAA 2006-231, January, 2006.

[5]Langelaan, J., "Biologically Inspired Flight Techniques for Small and Micro Unmanned Aerial Vehicles," *Proceedings of the 2008 AIAA Guidance, Navigation and Control Conference and Exhibit*, No. AIAA 2008-6511, Honolulu, HW, August 2008.

[6]Watkins, S., Milbank, J., Loxton, B., and Melbourne, W., "Replication of Atmospheric Conditions for the Purpose of Testing MAVs. MAV Flight Environment Project," Tech. rep., 2005.

[7]Hoffmann, G. M., Waslander, S. L., Huang, H., and Tomlin, C. J., "Autonomous Quadrotor Helicopter Testbed Design, Control, and Experiments," *submitted to AIAA Journal of Guidance, Control and Dynamics*, May 2008.

[8]Aeryon Labs Inc., 2009, 584 Colby Dr, Unit 1, Waterloo, ON, Canada, http://www.aeryon.com.

[9]Hoblit, F., *Gust Loads on Aircraft: Concepts and Applications*, AIAA Education Series, 1988.

[10]Greenwood, D. T., *Principles of Dynamics*, Prentice Hall, Upper Saddle River, NJ 07458, 2nd ed., 1988.

[11]Leishman, J. G., *Principles of Helicopter Aerodynamics*, Cambridge University Press, New York, NY, 2000, pp. 36–71.

[12]Thrun, S., Burgard, W., and Fox, D., *Probabilistic Robotics*, The MIT Press, Cambridge, MA, USA, 1st ed., 2005.

[13]Military Specification, "Flying Qualities of Piloted Airplanes," Tech. Rep. U.S. Military Specification MIL-F-8785C.

[14]Etele, J., "Overview of Wind Gust Modelling with Application to Autonomous Low-Level UAV Control," Tech. rep., Defence Research and Development Canada - Ottawa, November 2006.

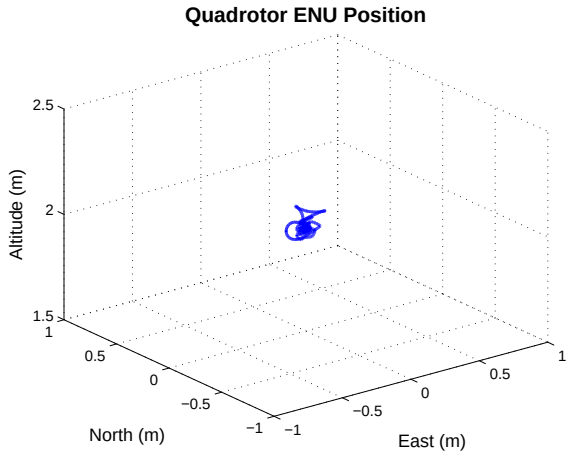

a)

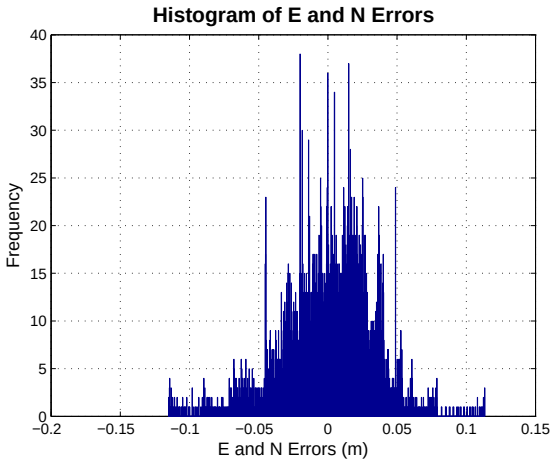

b)

Figure 7. Hover performance with PID,DD control and a wind compensation term for wind disturbance prediction rejection. a) Vehicle motion in three dimensions, b) histogram of errors in the horizontal plane (north,east).

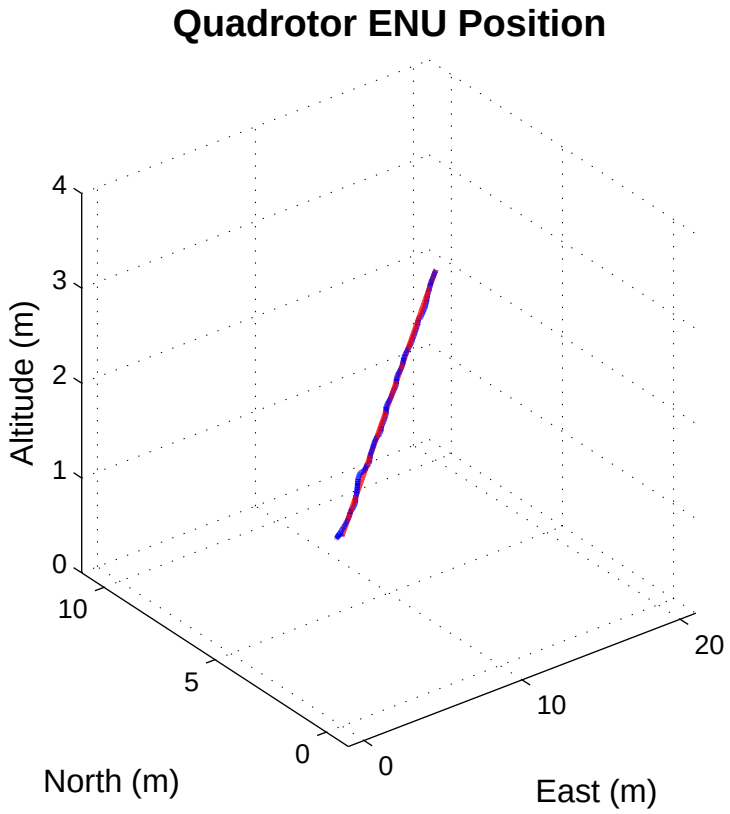

a)

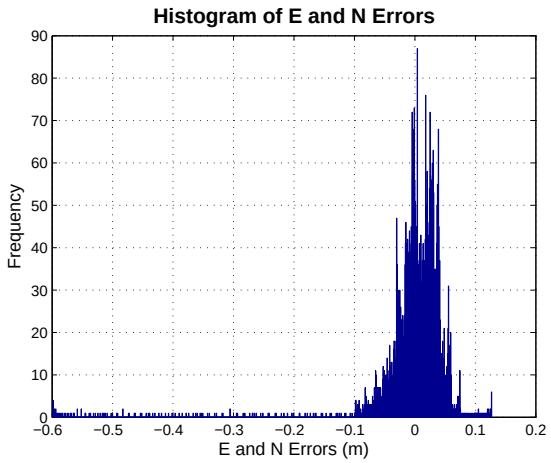

b)

Figure 8. Trajectory tracking of a straight path in windy conditions. a) Vehicle motion in three dimensions, b) histogram of errors in the horizontal plane (north,east).

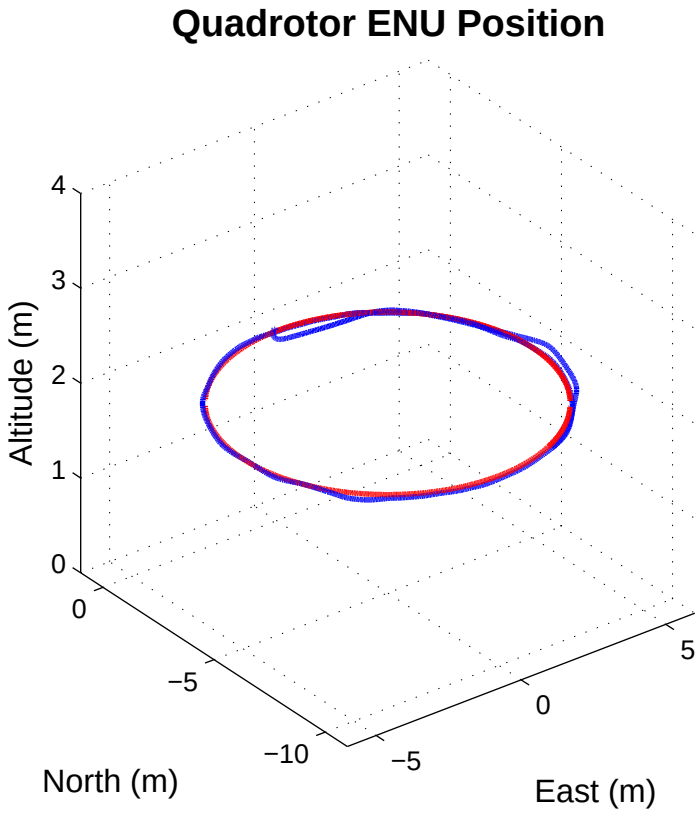

a)

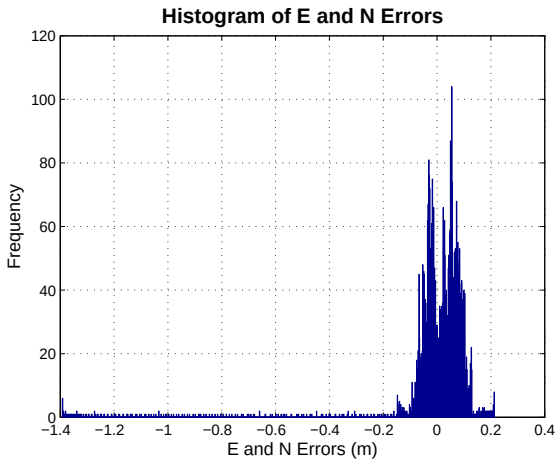

b)

Figure 9. Trajectory tracking of a circular path in windy conditions. a) Vehicle motion in three dimensions, b) histogram of errors in the horizontal plane (north,east).